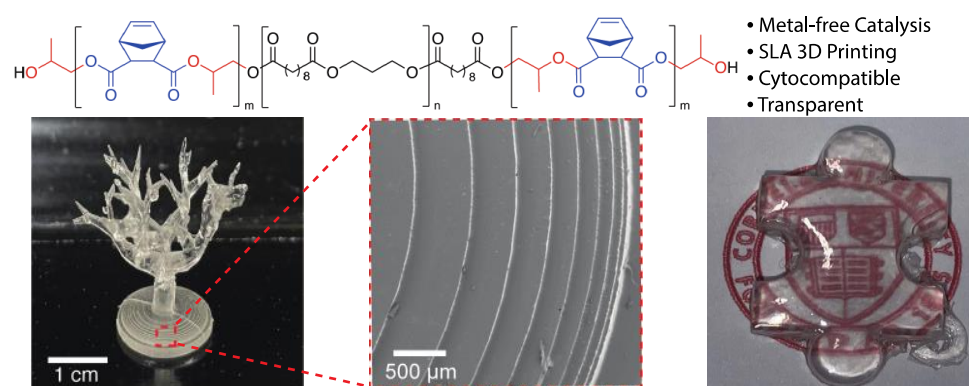# Cytocompatible, Transparent, and Clickable Resin for 3D Printing

Warrick Ma[#] and Yadong Wang[#]*

\#   Meinig School of Biomedical Engineering, College of Engineering, Cornell University, Ithaca, New York 14853-1801, United States

KEYWORDS. Ring-opening copolymerization; click chemistry; 3D printing resin; organ-on-a-chip; thiol-ene

GRAPHICAL ABSTRACT:

ABSTRACT. Stereolithography (SLA) has revolutionized the aerospace and automotive industry by rapidly prototyping irregularly shaped parts and tools on demand with high efficiency and resolution. In biomedical engineering, SLA has seen its nascent applications in areas such as tissue engineering and dentistry. All commercial SLA resins, however, have poor biocompatibility that prevents their broader acceptance in biomedical applications. For instance, the fabrication of bio-microfluidics, especially 3D organ-on-a-chip, still widely uses soft lithography and micro molding, although SLA would have been faster, cheaper, and have higher precision in the z-axis. This has prompted the advent of several thiol-ene

resins with good biocompatibility and tunable mechanical properties. However, the lack of commercial interest in thiol-ene resins highlights the need for more research with a focus on scalability, affordability, and versatility. Herein, we report a metal-free ring-opening copolymerization (ROCOP) to produce an ABA block copolyester on a 30-gram scale, which is unprecedented in the field of metal-free ROCOP. The synthetic strategy uses affordable cyclic anhydrides and epoxides to chain extend polypropylene sebacate—a polyester synthesized via polycondensation. This bridges the long-standing dichotomy between ring-opening copolymerization and polycondensation and enables the scalable synthesis of a thiol-ene resin (BC1). The 3D-printed materials are cytocompatible as well as optically transparent and have a 25 μm resolution. Furthermore, we can vary the mechanical properties by controlling the block lengths in the triblock structure. We believe that BC1, and more importantly the synthesis platform, will accelerate the discovery of biocompatible resins urgently needed for organ-on-a-chip and other biomedical devices.
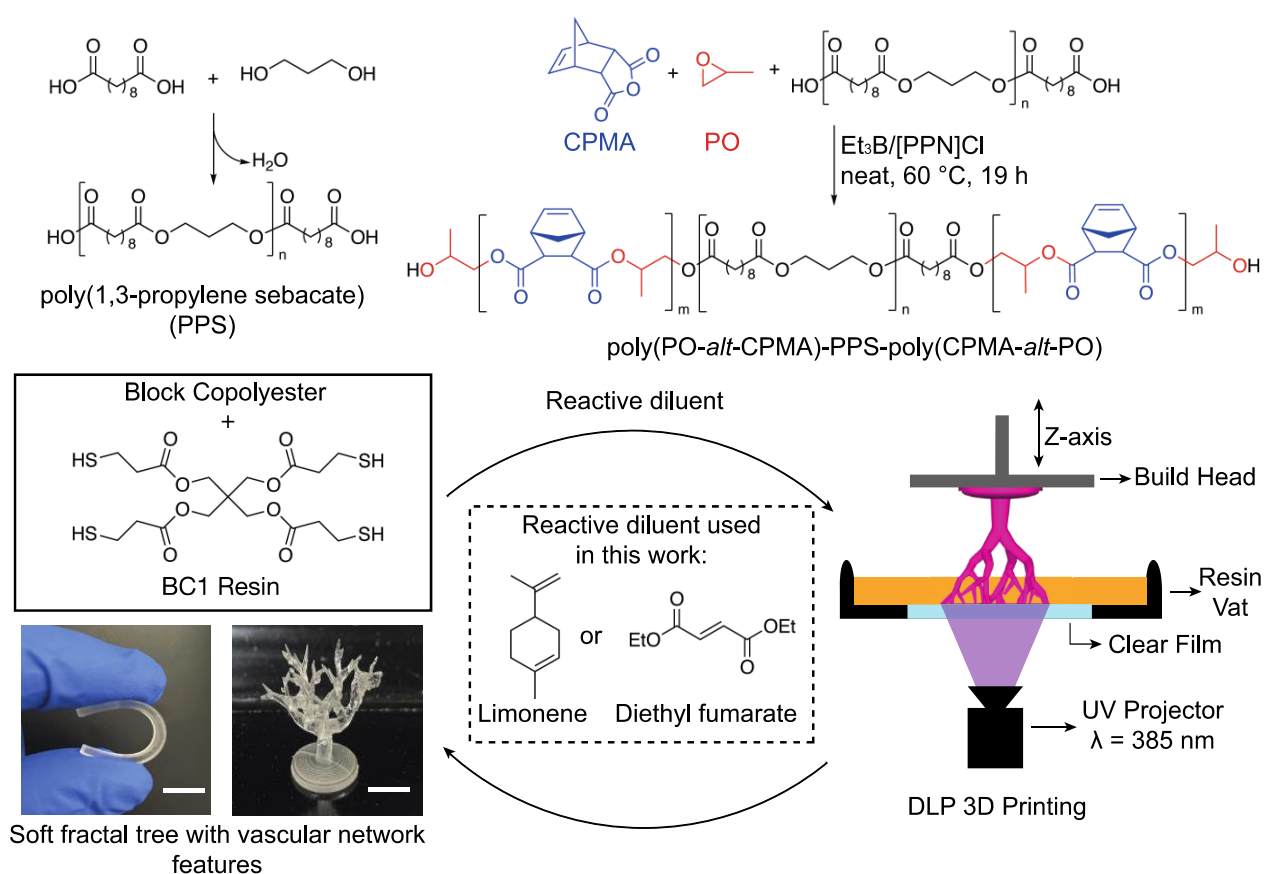
Introduction:

In September 2021, the European Union voted overwhelmingly in support of eventually phasing out animal use for research and education.[1] Organ-on-a-chip, a class of microfluidic devices, is a good candidate to replace animal models in the future because it can simulate physiological conditions using human cells in a highly-controlled environment.[2] There is a major barrier to the eventual replacement of animal models by organ-on-a-chip: its fabrication cannot be scaled up to satisfy the high demand for animal models. 3D microfluidics fabrication commonly uses soft lithography of polydimethylsiloxane (PDMS) that requires meticulous alignment and bonding of individual PDMS layers, thereby drastically increasing the processing time and difficulty, and reducing precision.[3-5] Moreover, stacking PDMS layers to achieve a 3D structure significantly increases the thickness between the layers, impeding mass transfer and limiting cell-cell contact.

SLA 3D printing can increase the manufacturability of microfluidic devices, but the toxicity of SLA resins hinders their acceptance in medicine. Almost all commercial resins are monomeric and/or oligomeric acrylates and methacrylates.[6] Leachates from commercial resins cause significant cell death

in vitro and *in vivo,* and a near 100% mortality of zebrafish embryos within 24 hours of incubation.[3, 7] Although post-printing treatments such as extensive washing, UV post-curing, heat treatment, and coating with biocompatible materials ameliorate some of the toxicity concerns, [3, 7, 8] it is highly beneficial to create a resin with inherent cytocompatibility, especially when the residual resin in microchannel cannot be efficiently removed by solvent washing.[3]

Here we used the high degree of control of metal-free, Lewis pair catalyzed ROCOP to produce BC1, a stable resin with rapid photo-crosslinking through thiol-ene click chemistry. 3D-printing of the resin via digital light processing (DLP) produced structures with good mechanical properties, cytocompatibility, transparency, and fine resolution. To our knowledge, this is the first example of polyesters synthesized via metal-free ROCOP in 3D printing. We believe that this strategy will expand the repertoire of biocompatible resins at scale and lead to functional materials with precisely controlled polymer architectures using biologically relevant diacid and diol monomers.

poly(1,3-propylene sebacate) (PPS)

CPMA   PO

Et₃B/[PPN]Cl
neat, 60 °C, 19 h

poly(PO-*alt*-CPMA)-PPS-poly(CPMA-*alt*-PO)

Block Copolyester
+

BC1 Resin

Reactive diluent

Reactive diluent used in this work:

Limonene   Diethyl fumarate

Z-axis
Build Head
Resin Vat
Clear Film
UV Projector
λ = 385 nm

DLP 3D Printing

Soft fractal tree with vascular network features

Scheme 1. A workflow illustrating the synthesis of poly(PO-*alt*-CPMA)-PPS-poly(CPMA-*alt*-PO), the formulation of BC1 resin, and its resultant DLP 3D printing (scale bar 1 cm). Et$_3$B: triethylborane; [PPN]Cl: bis(triphenylphosphine)iminium chloride; CPMA: cis-5-Norbornene-endo-2,3-dicarboxylic anhydride; PO: propylene oxide. (Double column artwork)

Materials and Methods

All chemicals were purchased from commercial sources and used without purification unless noted otherwise. All polymerizations were set up in a nitrogen-filled glovebox, then taken outside to stir in a silicon oil bath, and finally quenched by adding a small amount of ethanol. Propylene oxide (PO) was stirred over calcium hydride for three days and then vacuum transferred to a Straus flask for long-term storage in the glovebox. cis-5-Norbornene-endo-2,3-dicarboxylic anhydride (CPMA) was purified by vacuum sublimation at 70 °C. Bis(triphenylphosphine)iminium chloride ([PPN]Cl) was recrystallized by layering diethyl ether over a saturated solution of [PPN]Cl in dichloromethane (DCM). Scanning electron microscopy (SEM) was taken on JCM-7000 NeoScope Benchtop SEM.

Synthesis of PPS. A single-neck round bottom flask was charged with a stir bar, 1.05 eq of sebacic acid, and 1.0 eq of 1,3-propanediol. A distillation tube with a 0-4 Hi-vac valve was then attached to the flask and a receiving flask was connected to the other end. The assembled reaction apparatus was evacuated and refilled with nitrogen three times to remove oxygen and moisture. Afterward, it was put under a constant flow of nitrogen, first reacted at 120 °C for 24 hours then at 120 °C under vacuum for another 24 hours. Alternatively, it was reacted under nitrogen at 160 °C for three hours and then at 210 °C for two hours. We found that the second method yielded PPS with more consistent molecular weights.

ROCOP of CPMA and PO. To conduct small-scale ROCOP, CPMA and appropriate amounts of catalysts (see **Table 1**) were added into a dram vial with a stir bar in the glovebox, followed by adding PO with a syringe. The reactions were sealed with a Teflon cap that was further secured with electrical tapes. Vials were taken outside to stir at 60 °C for the desired amount of time. Large-scale ROCOP followed a similar procedure but was conducted in Schlenk bomb tubes sealed with Kontes valves. Conversions were calculated by integration of corresponding peaks in ^{1}H NMR spectrum of reaction

crude. Polymers were purified by precipitating in 1:1 water/ethanol mixture and subsequently dried under a high vacuum overnight. ^{1}H NMR spectra of purified samples (Figure S1-S7) were then recorded to analyze if homopolymerization of PO occurred.

Polymer characterization. NMR spectra were recorded on a Bruker AV III HD, 500 MHz) spectrometer with a broadband Prodigy cryoprobe or Varian IVarian INOVA 400, 400 MHz) spectrometer. CDCl$_3$ was used as the NMR solvent. MALDI-TOF-MS analysis was performed on a Bruker AutoFlex Max MALDI-TOF Mass Spectrometer in linear mode. MALDI matrix was 2-[(2E)-3-(4-tert-Butylphenyl)-2-methylprop-2-enylidene]malononitrile (DCTB) and potassium trifluoroacetate (KTFA) was the ionizing agent. To prepare MALDI samples, 50 microliters of polymer solution (1 mg/mL in THF) was mixed with 100 microliters of KTFA solution (5 mg/mL in THF) and 400 microliters of DCTB solution (40 mg/mL in THF); this formula gave the best to signal to noise ratio. The sample solutions were then blotted to the target plate with capillary tubes and allowed to air dry for 15 minutes prior to MALDI analysis. The resultant mass spectra were processed and analyzed with Bruker Autoflex in linear mode. Gel permeation chromatography (GPC) was conducted using Malvern Panalytical OMNISEC GPC system (Malvern Instruments Ltd., Malvern, UK) via a refractive index detector and a column set of T6000 M and T3000 with THF as the mobile phase (1 mL/min flow rate). The polymers were dissolved in HPLC grade THF at 5.0 mg/mL and filtered through a PTFE syringe filter. Number average molecular weights (M_n), weight average molecular weights (M_w), and polydispersities ($Đ$) were determined according to polystyrene standards. Differential scanning calorimetry (DSC) was conducted on a TA Instruments Q1000 Modulated Differential Scanning Calorimeter. Specifically, a heat/cool/heat cycle was conducted and glass transition temperature ™ was measured on the final heating ramp. Thermogravimetric analysis (TGA) was conducted with a TA Instruments Q500 Thermogravimetric Analyzer to determine glass transition temperature (T_g), melting temperatures (T_m), and crystallization temperatures (T_c).

To prepare crosslinked block copolyesters for mechanical and thermal testing, polymer solution in propylene carbonate was spread in a mold and UV-cured by a handheld UV lamp (long wave) for one

minute with pentaerythritol tetrakis(3-mercaptopropionate) (PETMP) in the presence of diphenyl(2,4,6-trimethylbenzoyl)phosphine oxide (TPO). Propylene carbonate was removed via sequential washing in ethanol with 75%, 50%, and 25% propylene carbonate, and eventually pure ethanol. Residual ethanol was then removed *in vacuo*. Tensile testing bars were then cut out with a die. Tensile testing and cyclic testing were conducted at room temperature on Instron 5943 equipped with 50 N loading cell and Bluehill Universal software. To prepare samples for photorheology, a solution was prepared similarly to the above. Photorheology was conducted at room temperature on a TA Instruments DHR3 Rheometer equipped with a UV curing accessory; the geometry was 20 mm parallel plate, composed of a disposable aluminum upper plate and an acrylic lower plate. A 365 nm UV filter was used, and the power output was 30 mW.

Cytocompatibility Study. The study was conducted according to a previously reported procedure with slight alterations.[9] Specifically, human umbilical vein endothelial cells (HUVECs) grown in Endothelial Cell Growth Medium MV2 (Promocell #39221) were used. For the toxicity assay, cells were seeded at 10,000 per well in a 96-well plate. Sample from entry 6, table 1 (18 wt% PPS) was cured with PETMP and the solvent was removed as described in the previous section.

BC1 Resin preparation and 3D Printing. For a large-scale ROCOP, 9.11 g of PPS, 15.1 g of CPMA, and 36 mL of PO were added to a Schlenk bomb flask in a nitrogen-filled glovebox. [PPN]Cl (1M in DCM) and Et$_3$B (1M in hexane), 0.92 mL each, were added to the mixture. The bomb flask was then sealed and taken outside to stir at 60 °C for 19 hours. The reaction was quenched with a small amount of ethanol and then mixed with 20 mL of limonene. Butylated hydroxytoluene (BHT) and TPO, 675 mg each, were dissolved together in 5 mL of acetone and the solution was added to the resin mixture. Resins were then stirred in open air away from light to reach homogeneity, after which resins could be printed directly without removing excess PO. If PO was evaporated *in vacuo*, a proper amount of polar solvents such as ethyl acetate and acetone should be added to lower the viscosity of resins. Lastly, PETMP was added to the mixture, which was then stirred briefly to acquire a homogenous and viscous solution. 3D printing was conducted on an Asiga Max 3D printer equipped with a 385 nm light source and each layer was printed with a 5 second exposure and at maximum intensity. For post-processing, printed objects

were briefly washed with acetone, followed by an extensive wash in isopropanol to remove uncured resins, and then post-cured in Asiga Flash UV chamber.

Results and Discussions

PPS Synthesis and Characterization. Our prior work on DLP resins derived from acrylate-functionalized poly(glycerol sebacate)[10] indicate that sebacate would impart elasticity because sebacic-based polyesters possess a flexible octamethylene chain. Furthermore, sebacic acid has been used as a monomer for materials approved for drug delivery by the US FDA.[11] However, direct condensation of sebacic acid with photocrosslinkable monomers is impractical because of the high temperature required (120°C to 220°C). Chain extension of polyesters under mild conditions circumvents this limitation and enables direct functionalization of aliphatic polyester by many reactive functional groups. Specifically, Lewis-pair-catalyzed ring-opening copolymerization (ROCOP) of cyclic anhydrides and epoxides directly incorporates diverse functional groups from commercially available monomers, producing perfectly alternating block copolyesters with good molecular weights ($M_n > 10$ kDa) and low dispersity ($Đ < 1.3$).[12] Lewis pair catalysts that are compatible with protic chain transfer agents (CTAs) enable this by chain extension of CTAs and sequential addition approaches.[13, 14-17]

We synthesized PPS macroCTA by melt condensation of 1.05 eq of sebacic acid and 1 eq of 1,3-propanediol (Scheme 1). The 0.05 eq excess is empirically chosen to compensate for the sublimation of sebacic acid. PPS comprised a series of low molecular weights oligomers (Figure 1) according to GPC. We confirmed melt condensation's lack of end group control by observing three species in decreasing abundance via MALDI-TOF: α-COOH-ω-COOH-PPS, α-OH-ω-COOH-PPS, and α-OH-ω-OH-PPS (Figure S8). Because previous research showed that COOH and OH initiate ROCOP in similar manners,[12] PPS is represented as having COOH end groups for simplicity (Scheme 1).

Catalyst Choice. We originally intended to use a recently developed bifunctional aminocyclopropenium aluminum catalyst abbreviated as **AlCl**,[12, 18] because the practical use of ROCOP

catalyzed by widely used metal catalysts has only been sparingly explored.[19] Unlike Et_3B/[PPN]Cl binary system where the Lewis acid and Lewis base are distinct molecules, **AlCl** contains covalently tethered Lewis acid and Lewis base that maintain catalyst activity in diluted polymerization medium and prevents inhibition by protic CTAs.[12, 18, 20] We initially deemed **AlCl** suitable because we wanted to incorporate high-weight percentages of PPS in the block copolymer. While **AlCl** produced block copolyester with 10 wt% of PPS (M_n = 8.9 kDa, $Đ$ = 1.14) and 18 wt% of PPS (M_n = 5.4 kDa, $Đ$ = 1.22), the residual catalyst was extremely difficult to remove despite repeated precipitation and ion exchange columns. Moreover, **AlCl** triggered thiol-ene crosslinking in ten minutes without UV exposure, rendering it unusable as a resin.

Table 1. poly(PO-*alt*-CPMA)-PPS-poly(CPMA-*alt*-PO) synthesized by ROCOP (Double column table)

entry[a]	PPS wt%[b]	[CPMA]:[PO]:[PPS]:[Et_3B]:[[PPN]Cl][c]	M_n (kDa)[d]	$Đ$[d]	T_g (°C)[e]	T_m/T_c (°C)[e]
1	100%	N/A	2.9	1.84	N/A	52/28
2	61%	100:600:12:1:1	3.2	1.54	-23	49/17
3	50%	100:600:7.6:1:1	4.0	1.44	-43	44/-2
4	37%	100:600:4.5:1:1	5.0	1.40	-35	39/NA
5	31%	100:600:3.2:1:1	5.4	1.30	-14	NA
6	18%	100:600:1.6:1:1	7.2	1.24	21	NA

[a]PPS and poly(PO-*alt*-CPMA)-PPS-poly(CPMA-*alt*-PO) were synthesized according to **Scheme 1**. The number in all subscripts represents the weight percentage of PPS (M_n = 2.9 kDa, $Đ$ = 1.84) relative to ring-opened CPMA and PO at full CPMA conversion.
[b]Conversion was equivalent to the percentage of ring-opened CPMA and was determined by ^{1}H NMR at the 19th hour of polymerization—all entries reached 100% conversion except for entry 2 (61 wt% PPS) which reached 88% conversion.
[c]Small-scale reactions were set up with 3 mmol of CPMA.
[d]Determined by GPC in THF, calibrated with polystyrene standards.
[e]Determined by DSC; NA: Not observed.

Further, the brightly colored **AlCl** stained the polymers such that they would interfere with microscopic analysis that is critical for organ-on-a-chip. Additionally, the use of metals such as Al, Co, and Cr severely limits metal-catalyzed ROCOP's applications in food packaging and medicine.[18, 21, 22] The recent advent of boron-based Lewis-pair catalyzed ROCOP alleviates the toxicity concern and has

demonstrated potential in drug delivery and biological imaging.[16] To produce colorless materials that would not undergo uncontrolled crosslinking, we therefore used a Et$_3$B/[PPN]Cl binary catalyst system. Further, the catalyst pair has wide substrate scope, good biocompatibility, and good affordability. The resultant poly(PO-*alt*-CPMA)-PPS-poly(PO-*alt*-CPMA) at 18 wt% of PPS (entry 1, Table 1) has higher molecular weight than that produced by **AlCl**.

PPS Mediated ROCOP is an immortal polymerization. The dependence of M_n and dispersity on PPS equivalence is consistent with the immortal nature of the polymerization. M_n negatively correlates with PPS equivalence (Table 1), confirming PPS underwent efficient chain transfer to afford poly(PO-*alt*-CPMA)-PPS-poly(CPMA-*alt*-PO). In agreement with previous reports of Et$_3$B/[PPN]Cl catalyzed ROCOP with or without small molecule CTAs, anhydride conversion increases linearly with M_n and time (Figure 1A-B), validating linear and uniform chain extension from PPS.[16, 17] The conversion-M_n best-fit curve intercepts the y-axis at 2323 g/mol, approximating the M_n of PPS and suggesting the absence of epoxide homopolymerization (Figure 1A). Similar to other reported protic CTAs used in ROCOP catalyzed by binary catalyst systems,[23] high PPS loadings decrease polymerization rates: polymerization with 18 wt% PPS (entry 6, Table 1) reached complete conversion in five hours, while the one with 61 wt% PPS reaching only 88% conversion in 19 hours (entry 2, Table 1). It is likely that high PPS loadings inhibit catalyst activity due to increased reaction viscosity, dilution of the active catalytic species, and/or competition with binding of the growing anionic chain to the active catalytic species. Notably, M_n of poly(PO-*alt*-CPMA)-PPS-poly(CPMA-*alt*-PO) is significantly lower than their theoretical M_n calculated via stoichiometry ratios in Table 1. The presence of low molecular weight PPS species (Figure 1C) and potential side products, such as cyclic macromers resulting from backbiting or anhydride from the condensation of two carboxylic acids, possibly result in the large discrepancy. In contrast, small molecule CTAs and oligomeric CTAs with narrow dispersity ($Đ$ < 1.1) can achieve good agreement between the experimental and theoretical M_n because they have well-defined structures and discrete molecular weights enabling precise calculation of their concentrations. On the same note, the high dispersity ($Đ$ = 1.82) and

ill-defined structure of PPS makes it difficult to calculate its molar concentration to study the exact inhibition mechanism.[12]

Characterization of poly(PO-*alt*-CPMA)-PPS-poly(CPMA-*alt*-PO). The absence of ether linkages indicates that only alternating copolymerization of CPMA and PO occurred (Table 1, Figure 2A, Figure S1-S5). Notably, poly(PO-*alt*-CPMA)-PPS-poly(CPMA-*alt*-PO) with 31 wt% of PPS synthesized
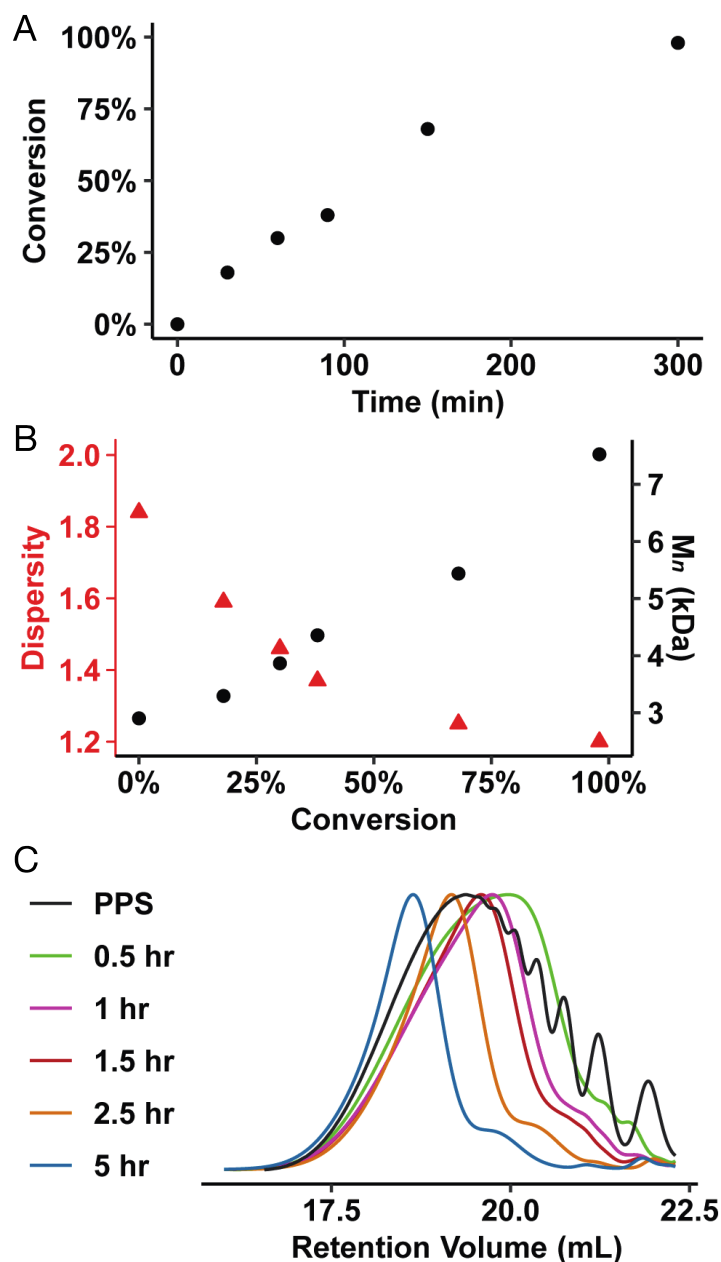

Figure 1. Kinetics of the synthesis of poly(PO-*alt*-CPMA)-PPS-poly(CPMA-*alt*-PO) with 18 wt% PPS. A, B) Progression of conversion of CPMA (determined by ^{1}H NMR), $Đ$, and M_n during the reaction. C) GPC traces of aliquots throughout the synthesis showing $Đ$ decreasing and molecular weights increasing. (Single column artwork)

on a 30-gram scale has higher molecular weights ($M_n = 8.2$ kDa) and lower dispersity ($Đ = 1.20$) compared

to its small-scale equivalent (entry 5, Table 1). This improvement in polymerization performance likely results from Schlenk bomb's superior air-free environment compared to that of vials and the more accurate addition of Et$_3$B and [PPN]Cl at a large scale. Meanwhile, weighing [PPN]Cl crystals directly to the reaction mixture at a small scale caused noticeable polyether formation and low CPMA conversion at high PPS concentrations (50 wt% and 61 wt%), likely due to a higher likelihood of inexact ratios of Et$_3$B relative to [PPN]Cl enabling Et$_3$B-mediated homopolymerization.[15, 24] Stereochemistry analysis with ^{1}H NMR spectrum shows that 10% of ring-opened CPMA have adopted a trans conformation, and varying concentrations of PPS have no effect on the stereoselectivity (Figure 2C). Prolonged incubation in excess PO likely causes the observed stereoirregularity.[14] Diffusion NMR shows one diffusion coefficient for all proton signals, suggesting that the PPS has chain-extended to produce poly(PO-*alt*-CPMA)-PPS-poly(CPMA-*alt*-PO) (Figure 2B). MALDI-TOF of poly(PO-*alt*-CPMA)-PPS-poly(CPMA-*alt*-PO) with 50 wt% and 61 wt% of PPS (entry 2 and 3, Table 1) confirmed its ABA triblock architecture furnishing uniform propanol chain ends with a distribution of block lengths (Figure 3). The observed mass values account for all three possible microstructures that resulted from three different end-group combinations of PPS (Figure S9, S10). Gaussian distributions within each cluster indicates a statistical distribution of different amounts of sebacate-propanediol units and CPMA-PO units (Figure S10). We attributed 2417 m/z to three possible species: [α-OH-ω-COOH-(PPS)$_4$]-*block*-(PO-*alt*-CPMA)$_6$, [α-OH-ω-OH-(PPS)$_4$]-*block*-(PO-*alt*-CPMA)$_6$, and [α-COOH-ω-COOH-(PPS)$_3$]-*block*-(PO-*alt*-CPMA)$_6$ (Figure S10, Table S1). The identification of 2438 m/z validated our tabulated analysis (Table S2). We did not observe any polyether segment or chloride-initiated chain because they could not afford the observed mass patterns.

A high catalyst loading (18 wt% PPS, entry 6, Table 1) produces the desired block copolyester, but also leads to chloride-initiated chains. Its GPC chromatogram shows a low molecular weight shoulder (Figure 1C, Figure 2D). In addition, MALDI- TOF of the crude reaction mixture quenched at low conversion reveals both chloride-initiated chains and PPS-initiated chains in (Figure S12). Diffusion NMR at full conversion reveals two polymeric species, consistent with the presence of low molecular weight chloride-initiated species (Figure S7). In contrast, higher equivalents of PPS loading have

minimized the probability of chloride-initiated species chain extending to any significant degree: GPC chromatogram of entry 5, Table 1 (31 wt% PPS) and entry 4, Table 1 (37 wt% PPS) does not contain any low molecular weight shoulder (Figure 1D)—and diffusion NMR of entry 5, Table 1 (31 wt% PPS) displays a unimodal distribution of diffusion coefficient (Figure 1B).

The dispersity of the copolyesters after chain extension is lower than that of PPS and decreases as PPS equivalent increases (Table 1). To understand this trend, we tracked the progression of dispersity during the polymerization of entry 6, Table 1 (18 wt% PPS). The polymer dispersity decreases as the polymerization proceeds (Figure 1). In ROCOP conducted with small-molecule CTAs, dispersity is generally invariant with the degree of polymerization and a low dispersity is maintained due to rapid equilibration between anionic chain ends and protic species. Further, the few examples of ROCOP conducted with macroCTA's used commercially available polymers with narrow dispersity.[12] We therefore surmise that this downward trend of dispersity stems from a diffusion-controlled chain transfer mechanism. It is likely that PPS with lower-molecular weight chain-extends more rapidly. This mechanism preferentially decreases the abundance of low molecular weight species, subsequently decreasing the dispersity. Indeed, the progression of molecular weight with time (Figure 1) for entry 6, Table 1 (18 wt% PPS) shows that low molecular weight PPS oligomers were consumed within 30 minutes.
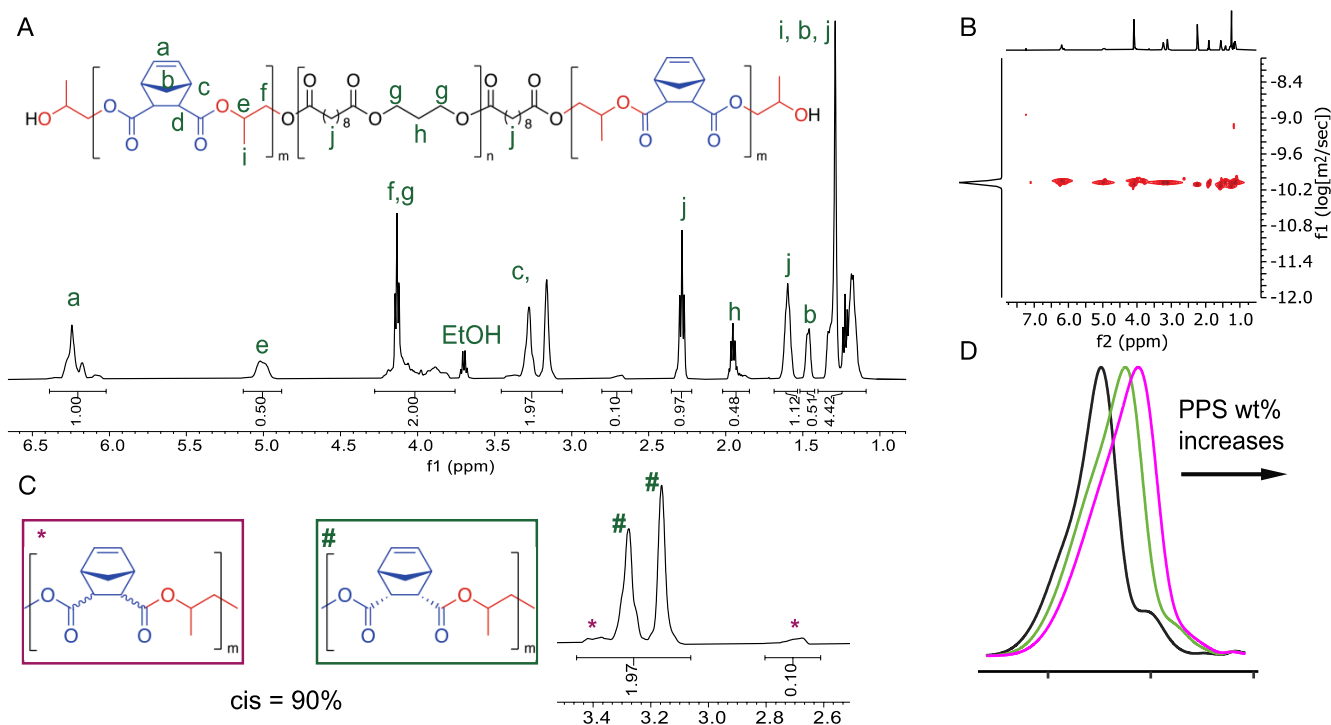
Figure 2. NMR (CDCl₃, 500 MHz) and GPC Analysis of poly(PO-*alt*-CPMA)-PPS-poly(CPMA-*alt*-PO). A) ^{1}H NMR of poly(PO-*alt*-CPMA)-PPS-poly(CPMA-*alt*-PO) with 31 wt% PPS synthesized on a 30-gram scale; B) Diffusion NMR of the previous sample showing all proton signals had the same diffusion coefficient (two peaks with higher diffusion coefficients are from solvents); C) Stereochemistry analysis of poly(PO-*alt*-CPMA)-PPS-poly(CPMA-*alt*-PO); D) GPC traces of poly(PO-*alt*-CPMA)-PPS-poly(CPMA-*alt*-PO) synthesized at various PPS concentrations (entry 4-6, Table 1). (Double column artwork)

Lastly, PPS is absent in MALDI-TOF of entry 6, Table 1 (18 wt% PPS) quenched in 30 min, which corroborates with the observation that PPS is an efficient CTA.

This synthesis strategy bridges the dichotomy between ROCOP and polycondensation, providing access to polyesters that cannot be synthesized via ROCOP or polycondensation alone. Notwithstanding its broad substrate scope, ROCOP requires cyclic anhydrides. However, many biologically relevant diacids such as ketoglutaric acid, adipic acid, and sebacic acid, cannot form cyclic anhydrides. Furthermore, for biologically relevant diacids with commercially available anhydrides (such as succinic anhydride, glutaric anhydride, tartaric anhydride, and itaconic anhydride), they are either too sluggish to react or, in the case of itaconic anhydride, have acidic protons that are incompatible with the growing alkoxide chain ends during ROCOP process. On the other hand, polycondensation can incorporate these diacids, but its harsh reaction condition often causes degradation or premature crosslinking of reactive
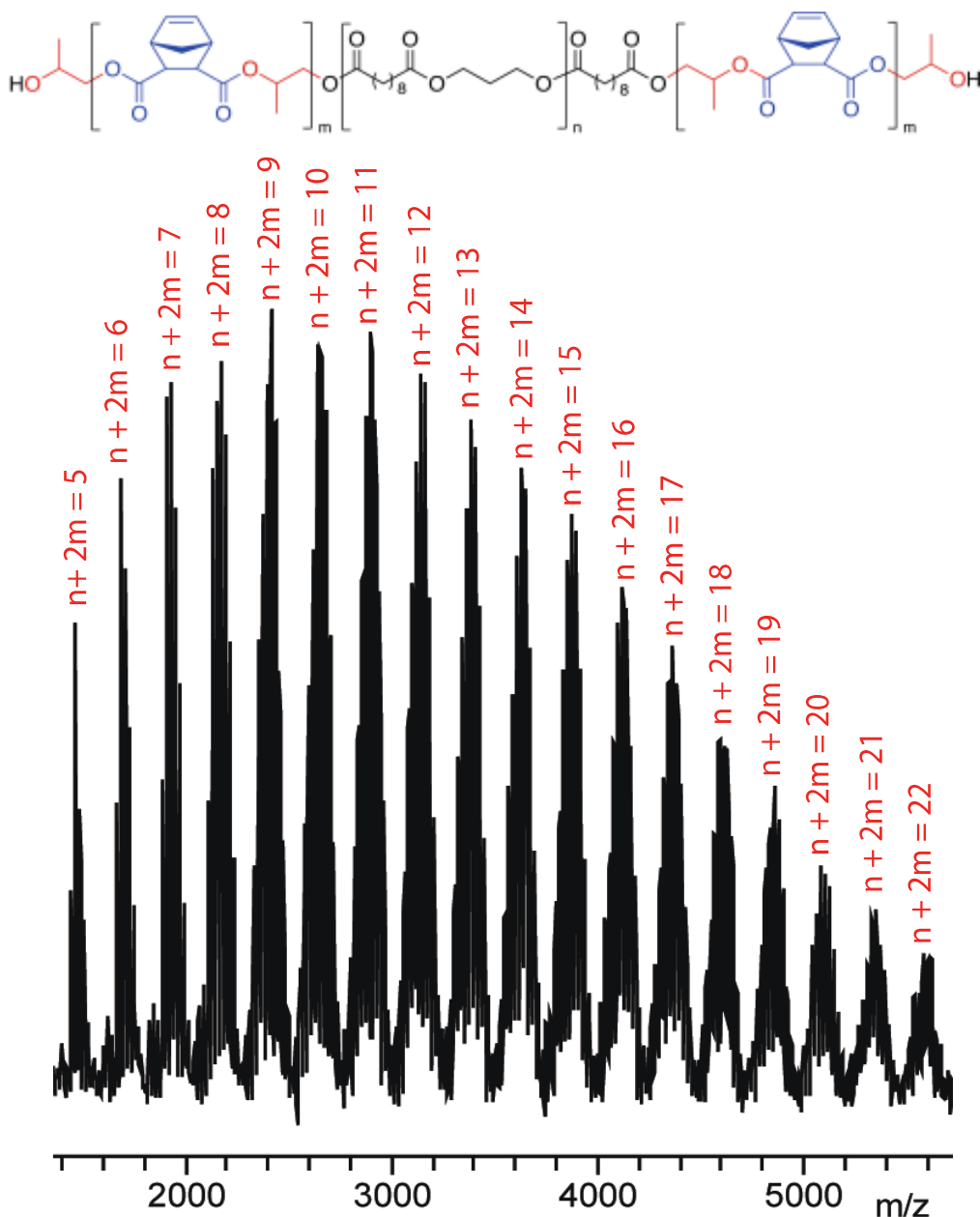
Figure 3. MALDI-TOF of poly(PO-*alt*-CPMA)-PPS-poly(CPMA-*alt*-PO)) with 61 wt% PPS. Only chains derived from α-COOH-ω-COOH-PPS is shown for simplicity, although observed mass values also account for triblock copolyester derived from α-OH-ω-OH-PPS or α-COOH-ω-OH-PPS (Figure S9) (Single column artwork)

functional groups, which manifests as large dispersity ($Đ$ = 1.7 -10) and batch-to-batch inconsistencies.[9, 25, 26] Sebacate-derived elastomers are therefore still commonly functionalized by reacting their reactive side chain (OH or COOH) with acyl chlorides, anhydrides, or carbodiimides, all of which needs a large amount of hazardous reagents.[10, 25, 27] Therefore, metal-free ROCOP and polycondensation serve as a good complement to each other in producing functional polyesters.

Thermal and Mechanical Properties of Block Copolyester with Various PPS Content. While alternating polyesters comprising of PO and tricyclic anhydrides have high T_g over 100 °C and no T_m,[23]
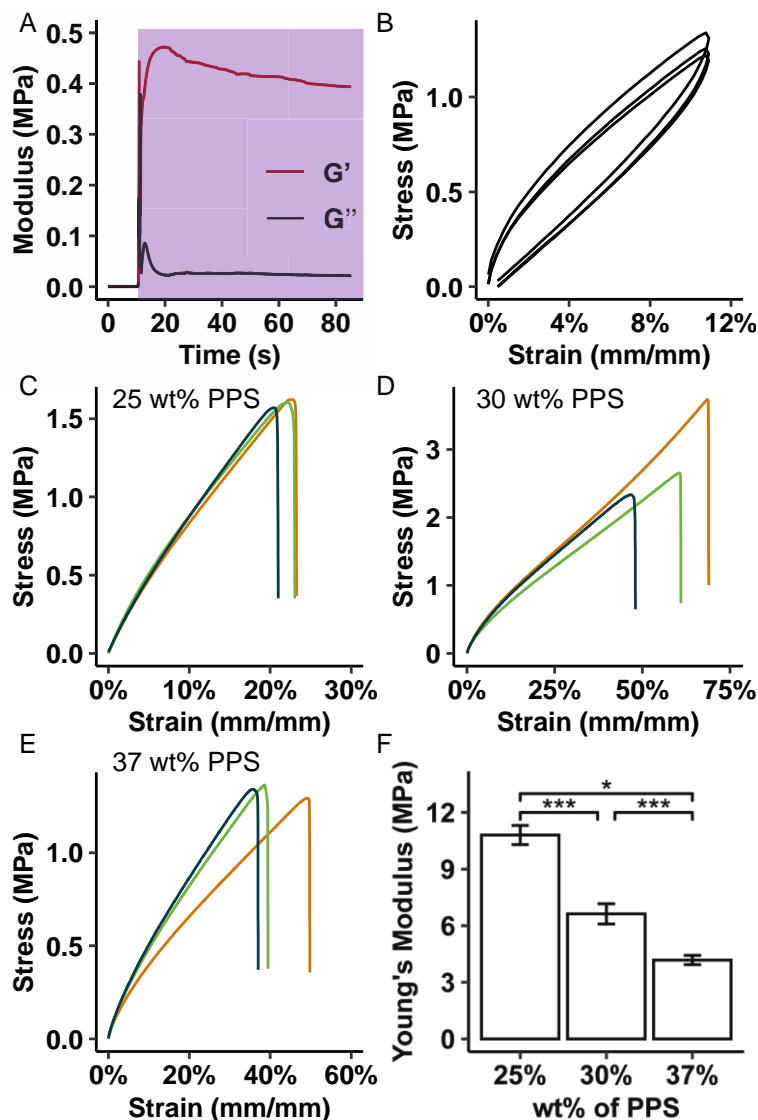
Figure 4. Mechanical testing of cured poly(PO-*alt*-CPMA)-PPS-poly(CPMA-*alt*-PO). A) Photocuring kinetics of entry 6, Table 1 cured by PETMP with TPO as the initiator; magenta box represents onset of UV exposure (385 nm, 3 W). B) Cyclic tensile testing of cured entry 6, Table 1 (18 wt% PPS) showing traces of cycle 1, cycle 25, and cycle 50. C-E) Tensile testing of various polymer samples (n=3). F) Comparison of Young's modulus derived from tensile testing. *p<0.05 ***p<0.001 (Single column artwork)

presumably because of rigidity of norbornene backbone and reactivity of double bonds at high temperatures, the octamethylene segment in the PPS soft block confers more flexibility and lowers the T_g of poly(PO-*alt*-CPMA)-PPS-poly(CPMA-*alt*-PO). All polymer samples' T_g are lower than 37 °C and negatively correlated to equivalents of PPS—although leftover CPMA likely has made entry 2, Table 1 (61 wt% PPS) an outlier—its T_g reverts the downward trend and is 20 °C higher than that of entry 3, Table 1 (50 wt% PPS, T_g = -43 °C). At higher equivalents of PPS (entry 2-4, Table 1), poly(PO-*alt*-CPMA)-PPS-poly(CPMA-*alt*-PO) adopts more PPS characters by displaying distinctive melting temperature (T_m)

and crystallization temperature (T_c) (PPS: T_m = 52 °C, T_c = 28 °C): T_m increases from 39 °C (entry 4, Table 1, 37 wt% PPS) to 49 °C (entry 2, Table 1, 61 wt% PPS) and T_c increases from -2°C (entry 3, Table 1, 50 wt% PPS) to 17 °C (entry 2, Table 1, 61 wt% PPS). Due to the reactivity of norbornene, increasing the length of the poly(PO-*alt*-CPMA) block has rendered poly(PO-*alt*-CPMA)-PPS-poly(CPMA-*alt*-PO) less

stable at high temperatures. Entry 3, Table 1 (50 wt% PPS) shows two-step degradation with the first onset at 223 °C and the second onset at 376 °C (Figure S19); PPS macroCTA has a single onset at 377 °C (Figure S18), and we therefore attribute the first onset of entry 3, Table 1 (50 wt% PPS) to poly(PO-*alt*-CPMA) block. We have observed similar stepwise degradation in entry 2, Table 1 (61 wt% PPS) but identified a minor transition at 151 °C attributed to leftover CPMA monomer (Figure S20). As the first degradation was not complete when the second degradation took place, we cannot derive the weight percentage of each block from TGA data.

Norbornene-functionalized polymers have been explored in 3D printing because of their facile thiol-ene crosslinking.[28, 29] We chose PETMP as the crosslinker due to its good biocompatibility in denture applications, low vapor pressure, and efficient generation of highly crosslinked thiol-ene networks.[22, 30, 31] Resin's storage modulus (G') and loss modulus (G'') rapidly increased upon exposure to UV (Figure 4A), indicating efficient crosslinking (Figure 4A). poly(PO-*alt*-CPMA)-PPS-poly(CPMA-*alt*-PO) crosslinked with PETMP were elastomeric and underwent cyclic loading and unloading (0-12% strain range) fifty times without breakage (Figure 4B). Furthermore, cycles 1, 25, and 50 exhibits nearly identical   elastic
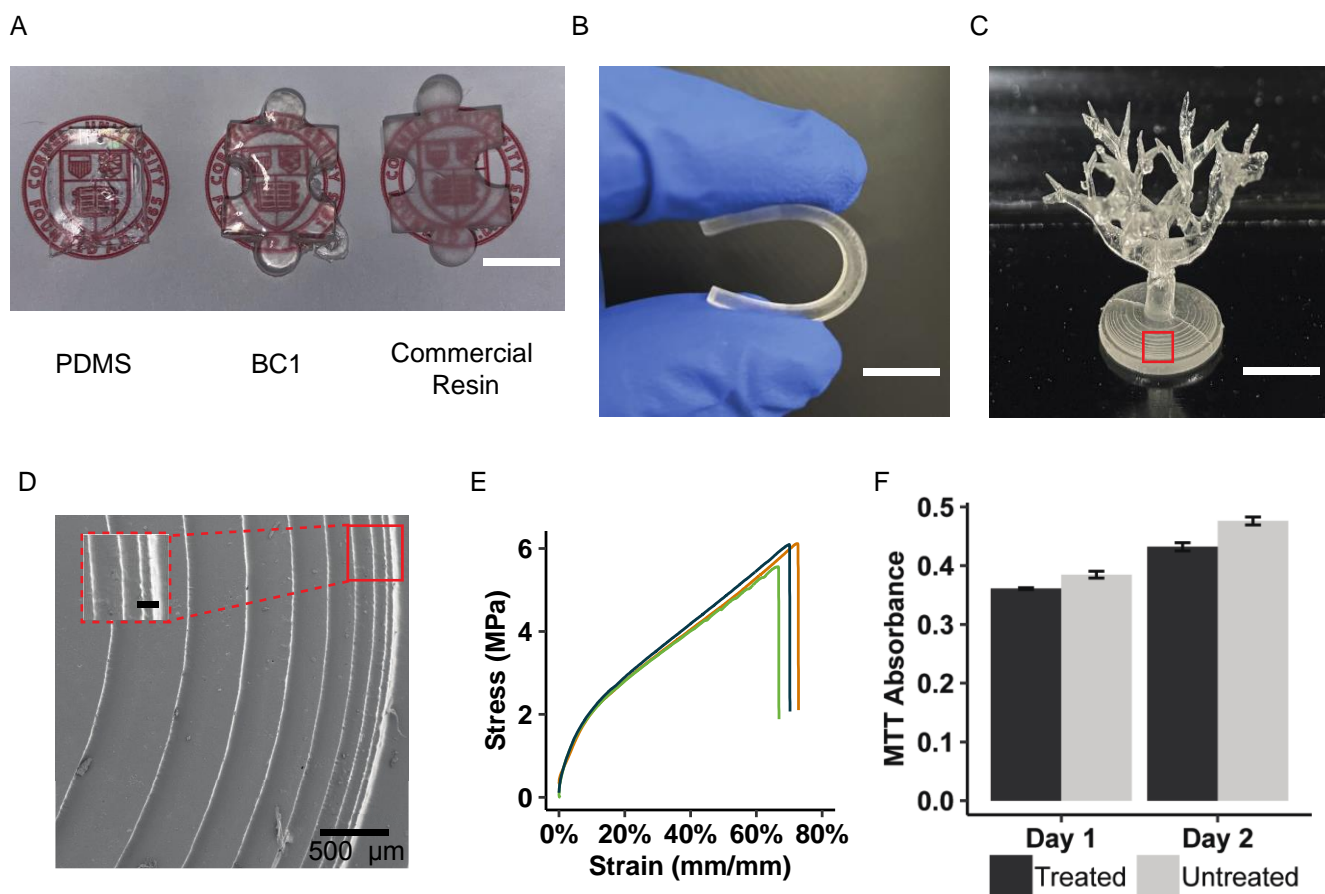
Figure 5. 3D Printing of BC1 formulated from poly(PO-*alt*-CPMA)-PPS-poly(CPMA-*alt*-PO) with 31 wt% PPS (M_n = 8.2 kDa, $Đ$ = 1.20). A) Comparison between PDMS, BC1, and commercial resin (Whip Mix VeriGuide OS). B) Printed dogbone sample undergoing mechanical distortion. C) A printed tree showing bifurcations with overhangs and smooth curvatures that are common in the mammalian vasculature. D) SEM image of highlighted area in figure C showcasing a 25 µm resolution (unlabeled scale bar: 50 µm) E) Mechanical testing of printed dogbone samples (n=3) F) *In vitro* cytocompatibility testing of poly(PO-*alt*-CPMA)-PPS-poly(CPMA-*alt*-PO) (entry 6, Table 1) cured with PETMP (n=4) with human umbilical vein endothelial cells (HUVECs); MTT absorbance linearly correlates to the number of viable cells. White scale bars: 1 cm. (Double column artwork)

behavior with very small hysteresis (Figure 4B). The increasing lengths of PPS block in poly(PO-*alt*-CPMA)-PPS-poly(CPMA-*alt*-PO) have decreased the crosslinking density and therefore Young's modulus (Figure 4F). The ultimate strain correspondingly increases from ε_{max} = 22 ± 0.3% for poly(PO-*alt*-CPMA)-PPS-poly(CPMA-*alt*-PO) with 25 wt% PPS to ε_{max} = 58 ± 4% for poly(PO-*alt*-CPMA)-PPS-poly(CPMA-*alt*-PO) with 31% PPS, although the one with 37 wt% PPS showed no significant difference to either (Figure 4C - 4E). It's important to note that poly(PO-*alt*-CPMA)-PPS-poly(CPMA-*alt*-PO) used for mechanical testing was made from another batch of PPS with molecular weights and dispersity different from those of PPS used for the kinetic study. Notwithstanding batch-to-batch variations of PPS,

these results confirm that our polymerization strategy allows us to tune mechanical properties by varying block lengths, a level of control that is difficult to achieve with step-growth polycondensation. The toughness and elasticity of the crosslinked materials encouraged us to pursue resins made of poly(PO-*alt*-CPMA)-PPS-poly(CPMA-*alt*-PO) and PETMP as suitable candidates for the 3D printing of soft materials.

DLP 3D-Printing of poly(PO-*alt*-CPMA)-PPS-poly(CPMA-*alt*-PO). Compared to acrylate-based resins, thiol-ene resins have increased biocompatibility, making them better candidates for fabricating bio-microfluidic devices.[22, 28, 31, 32] Many "ene" monomers have been used in biorthogonal chemistry (norbornene);[33] many natural metabolites (fumaric acid and itaconic acid) contain alkene bonds;[34] alkene bonds are also present in common food items (limonene).[35] Therefore, materials based on these molecules are likely biocompatible. The successful commercialization of thiol-ene resins (Ostemers) for fabricating organ-on-a-chip highlights their potential for success.[36] Although Ostemer resins are not designed for 3D printing,[37] many other proof-of-concept thiol-ene 3D printing resins have been reported in recent years.[35, 38, 39] Among them, polyester-based resins appeal to us the most because of their biodegradability,[40] tunable crosslinking density and mechanical properties,[38] and rapid gelation.[41] Furthermore, desirable functionalities can arise from advanced polyester architecture (diblock, triblock, star, hyperbranched etc.) that are impossible to access via monomeric or oligomeric resins.[12]

We investigated the printability of poly(PO-*alt*-CPMA)-PPS-poly(CPMA-*alt*-PO) with either 31wt% or 37wt% of PPS because they do not contain a significant fraction of chloride-initiated chains. Polymers' relatively high molecular weights require proper diluents to decrease the resin's viscosity to a printable value. Inert diluents such as propylene carbonate, ethyl acetate, and acetone caused poor xy resolutions and significant shrinkage stress during solvent removal. Therefore, we used limonene as the reactive diluent to formulate BC1. Limonene is renewably sourced, relatively safe for human consumption, and has been used in DLP resins with good printability and cytocompatibility.[30, 35, 42] 5s exposure per 100-μm layer consistently produced prints with high resolutions, whereas underexposure or overexposure caused prints to detach from the build platform or decreased xy resolutions. First, printed

BC1 shows good transparency and clarity similar to those of cured polydimethylsiloxane (PDMS) (Figure 5A), the staple polymer used to manufacture microfluidics and other biomedical implants.[4, 43] Second, objects of various structural complexity were printed according to our optimized parameters, demonstrating the versatility of our method (Figure 5B-5D). In particular, the tree structure (Figure 5B) demonstrates the BC1 has enough mechanical strength to form unsupported hierarchical structures with overhangs and smooth curvatures that are common in vascular trees.[44] The SEM image of the concentric rings resulting from layer-by-layer printing reveals a 25 μm resolution (Figure 5D). The resultant materials are much softer (E = 17.9 ± 0.4 MPa) than reported transparent resins used to print microfluidic devices and exhibit better transparency than commercial resins. Furthermore, DLP-printed dogbones reach their elastic limits at roughly 10% strain and display an ultimate strength of 5.21 ± 0.4 MPa at 67 ± 2% strain (Figure 5E). Lastly, thiol-ene cured block copolyester shows good cytocompatibility (viability > 70%) *in vitro* according to ISO 10993-2012(E)-Biological Evaluation of Medical Devices (Figure 5F). With these attributes, BC1 is a promising candidate for 3D printing biomaterials such as organ-on-a-chip and tissue scaffolds, which require superior cytocompatibility and fine resolutions.

We 3D-printed poly(PO-*alt*-CPMA)-PPS-poly(CPMA-*alt*-PO) with 37 wt% PPS with the same parameters, but all prints cracked promptly during washing with organic solvents. We hypothesize that because a longer PPS block length reduced crosslinking density and thus lower mechanical strength—the resultant shrinkage stress during drying would cause the crosslinked materials to crack and delaminate. Ongoing work includes optimizing resin compositions—especially the choice of reactive diluents and concentrations of polymers and crosslinkers—to 3D print poly(PO-*alt*-CPMA)-PPS-poly(CPMA-*alt*-PO) with higher PPS concentrations. We preliminarily studied the printability of the block copolyester with diethyl fumarate as the reactive diluent— at 2s exposure per 100-micron layer, the resultant resin was printed into dogbones with lower Young's modulus (E = 3.49 ± 0.23 MPa) and similar ultimate strain (ε_{max} = 73 ± 5%). We are thus confident that using other reactive dilutants with our polymer will yield materials with tunable mechanical properties.

Applying BC1 to 3D printing of microfluidic devices with improved biocompatibility will be a herculean undertaking that takes many iterations of optimizations and trial runs. To date, only certain commercial resins, and low molecular weight polypropylene glycol diacrylate have successfully printed microfluidic devices with microchannels. External factors such as printing settings, resin age, resin viscosity, and even humidity can affect the degree of curing and thus the concentration of uncured monomers/oligomers that can leach into their surroundings, thereby further complicating the development of biocompatible resins.[3] The promise of BC1, however, justifies the efforts needed to overcome these difficulties. In addition to its improved biocompatibility, thiol-ene resins yield uncreated alkene that can be further modified by click chemistry with functional biomolecules. One can adjust the degree of functionalization by adjusting the thiol/ene stoichiometric ratios—this is a layer of control impossible with acrylate-based resins because free radical crosslinking is uncontrollable. Furthermore, metal-free ROCOP's broad compatibility with anhydrides, epoxides, and protic CTAs will enable us to exploit the rich tapestry of possible polymer structures and functionalities. Currently, researchers can easily buy cyclic anhydrides furnishing alkenes, norbornenes, or phenyl groups; epoxides functionalized with propargyl groups, allyl groups, or aldehyde groups; and protic CTAs that span a wide range of molecular weights and physical properties. This list of monomers and CTAs already affords 45 explorable block copolymers. This number grows more as one adjusts the catalyst and CTA loading ratio to target various molecular weights, which drastically affects the performance and properties of resultant resins.

Conclusion

In this report, we bridge the dichotomy between polycondensation and ROCOP to afford BC1, a novel thiol-ene resin with good promises in biomedical engineering. The significance of our work is two-prong. First, we proved that metal-free ROCOP of cyclic anhydride and epoxides—in conjunction with melt condensation—can be scaled up to 30 grams while maintaining good control over end group identity and dispersity. This strategy combines the advantage of both polycondensation and ROCOP and readily accelerates the discovery of new materials without inventing new catalysts, monomers, or polymerization

methodologies. Second, ABA triblock copolyesters can be used as a photopolymer for 3D printing of materials with flexible mechanical properties, good optical transparency, and good cytocompatibility; ROCOP's compatibility with CTAs of vastly different chemical structures, as well as monomers of diverse functionalities, will meet the increasing demand for 3D-printed biomaterials with tailored properties and facile functionalization.

ASSOCIATED CONTENT

Supporting Information. The following files are available free of charge.

Supporting information containing NMR spectra, MALDI-TOF analysis, DSC traces, and TGA data (Supporting_info.pdf)

AUTHOR INFORMATION

Corresponding Author

Yadong Wang (yw839@cornell.edu)

Author Contributions

The manuscript was written through contributions of all authors. All authors have given approval to the final version of the manuscript.

Notes

The authors declare no conflict of interest.

ABBREVIATIONS

ROCOP, ring-opening copolymerization; CTA, chain transfer agent; NMR, nuclear magnetic resonance; GPC, gel permeation chromatography; DSC, dynamic scanning calorimetry; TGA, thermogravimetric analysis; MALDI-TOF, matrix-assisted laser desorption/ionization-time of flight mass spectrometry

REFERENCES

(1) Marshall, L. J.; Constantino, H.; Seidle, T. Phase-In to Phase-Out-Targeted, Inclusive Strategies Are Needed to Enable Full Replacement of Animal Use in the European Union. *Animals (Basel)* **2022**, *12* (7). DOI: 10.3390/ani12070863.

(2) van Berlo, D.; Steeg, E. V.; Amirabadi, H. E.; Masereeuw, R. The potential of multi-organ-on-chip models for assessment of drug disposition as alternative to animal testing. *Curr Opin Toxicol* **2021**, *27*, 8-17. DOI: 10.1016/j.cotox.2021.05.001.

(3) Musgrove, H. B.; Catterton, M. A.; Pompano, R. R. Applied tutorial for the design and fabrication of biomicrofluidic devices by resin 3D printing. *Analytica Chimica Acta* **2022**, *1209*, 339842. DOI: https://doi.org/10.1016/j.aca.2022.339842.

(4) Urrios, A.; Parra-Cabrera, C.; Bhattacharjee, N.; Gonzalez-Suarez, A. M.; Rigat-Brugarolas, L. G.; Nallapatti, U.; Samitier, J.; DeForest, C. A.; Posas, F.; Garcia-Cordero, J. L.; et al. 3D-printing of transparent bio-microfluidic devices in PEG-DA. *Lab Chip* **2016**, *16* (12), 2287-2294. DOI: 10.1039/c6lc00153j.

(5) Kuo, A. P.; Bhattacharjee, N.; Lee, Y. S.; Castro, K.; Kim, Y. T.; Folch, A. High-Precision Stereolithography of Biomicrofluidic Devices. *Adv Mater Technol-Us* **2019**, *4* (6). DOI: ARTN 1800395

10.1002/admt.201800395.

(6) Bagheri, A.; Jin, J. Photopolymerization in 3D Printing. *ACS Applied Polymer Materials* **2019**, *1* (4), 593-611. DOI: 10.1021/acsapm.8b00165.

(7) Carve, M.; Wlodkowic, D. 3D-Printed Chips: Compatibility of Additive Manufacturing Photopolymeric Substrata with Biological Applications. *Micromachines (Basel)* **2018**, *9* (2). DOI: 10.3390/mi9020091 From NLM PubMed-not-MEDLINE. Zhu, F.; Friedrich, T.; Nugegoda, D.; Kaslin, J.; Wlodkowic, D. Assessment of the biocompatibility of three-dimensional-printed polymers using multispecies toxicity tests. *Biomicrofluidics* **2015**, *9* (6), 061103. DOI: 10.1063/1.4939031 From NLM PubMed-not-MEDLINE. Rimington, R. P.; Capel, A. J.; Player, D. J.; Bibb, R. J.; Christie, S. D. R.; Lewis, M. P. Feasibility and Biocompatibility of 3D-Printed Photopolymerized and Laser Sintered Polymers for Neuronal, Myogenic, and Hepatic Cell Types. *Macromol Biosci* **2018**, *18* (7), e1800113. DOI: 10.1002/mabi.201800113 From NLM Medline. Ngan, C. G. Y.; O'Connell, C. D.; Blanchard, R.; Boyd-Moss, M.; Williams, R. J.; Bourke, J.; Quigley, A.; McKelvie, P.; Kapsa, R. M. I.; Choong, P. F. M. Optimising the biocompatibility of 3D printed photopolymer constructs in vitro and in vivo. *Biomed Mater* **2019**, *14* (3), 035007. DOI: 10.1088/1748-605X/ab09c4. Nejedla, Z.; Poustka, D.; Herma, R.; Liegertova, M.; Stofik, M.; Smejkal, J.; Sicha, V.; Kaule, P.; Maly, J. Class II biocompatible E-Shell 300 3D printing material causes severe developmental toxicity in Danio rerio embryos and reduced cell proliferation in vitro - implications for 3D printed microfluidics. *RSC Adv* **2021**, *11* (27), 16252-16267. DOI: 10.1039/d1ra00305d F. Macdonald, N. P.; Zhu, F.; Hall, C. J.; Reboud, J.; Crosier, P. S.; Patton, E. E.; Wlodkowic, D.; Cooper, J. M. Assessment of biocompatibility of 3D printed photopolymers using zebrafish embryo toxicity assays. *Lab on a Chip* **2016**, *16* (2), 291-297, 10.1039/C5LC01374G. DOI: 10.1039/C5LC01374G.

(8) Bhattacharjee, N.; Parra-Cabrera, C.; Kim, Y. T.; Kuo, A. P.; Folch, A. Desktop-Stereolithography 3D-Printing of a Poly(dimethylsiloxane)-Based Material with Sylgard-184 Properties. *Adv Mater* **2018**, *30* (22). DOI: 10.1002/adma.201800001.

(9) Ma, W.; Ding, X. C.; Chen, Y.; Wang, Y. D. Synthesis and Characterization of Alkyne-Functionalized Photo-Cross-Linkable Polyesters. *Acs Omega* **2022**, *7* (18), 15540-15546. DOI: 10.1021/acsomega.2c00272.

(10) Wu, Y. L.; D'Amato, A. R.; Yan, A. M.; Wang, R. Q.; Ding, X. C.; Wang, Y. D. Three-Dimensional Printing of Poly(glycerol sebacate) Acrylate Scaffolds via Digital Light Processing. *Acs Appl Bio Mater* **2020**, *3* (11), 7575-7588. DOI: 10.1021/acsabm.0c00804.

(11) Park, H.-s.; Seo, J.-a.; Lee, H.-Y.; Kim, H.-W.; Wall, I. B.; Gong, M.-S.; Knowles, J. C. Synthesis of elastic biodegradable polyesters of ethylene glycol and butylene glycol from sebacic acid. *Acta Biomaterialia* **2012**, *8* (8), 2911-2918. DOI: https://doi.org/10.1016/j.actbio.2012.04.026.

(12) Lidston, C. A. L.; Abel, B. A.; Coates, G. W. Bifunctional Catalysis Prevents Inhibition in Reversible-Deactivation Ring-Opening Copolymerizations of Epoxides and Cyclic Anhydrides. *J Am Chem Soc* **2020**, *142* (47), 20161-20169. DOI: 10.1021/jacs.0c10014.

(13) Gupta, P. K.; Pappuru, S.; Gupta, S.; Patra, B.; Chakraborty, D.; Verma, R. S. Self-assembled dual-drug loaded core-shell nanoparticles based on metal-free fully alternating polyester for cancer theranostics. *Mat Sci Eng C-Mater* **2019**, *101*, 448-463. DOI: 10.1016/j.msec.2019.03.041. Gupta, P. K.; Tripathi, S. K.; Pappuru, S.; Chabattula, S. C.; Govarthanan, K.; Gupta, S.; Biswal, B. K.; Chakraborty, D.; Verma, R. S. Metal-free semi-aromatic polyester as nanodrug carrier: A novel tumor targeting drug delivery vehicle for potential clinical application. *Materials Science and Engineering C-Materials for Biological Applications* **2020**, *107*.

10.1016/j.msec.2019.110285. Hu, L. F.; Zhang, C. J.; Wu, H. L.; Yang, J. L.; Liu, B.; Duan, H. Y.; Zhang, X. H. Highly Active Organic Lewis Pairs for the Copolymerization of Epoxides with Cyclic Anhydrides: Metal-Free Access to Well-Defined Aliphatic Polyesters. *Macromolecules* **2018**, *51* (8), 3126-3134. DOI: 10.1021/acs.macromol.8b00499. Kummari, A.; Pappuru, S.; Gupta, P. K.; Chakraborty, D.; Verma, R. S. Metal-free Lewis pair catalyst synergy for fully alternating copolymerization of

norborne anhydride and epoxides: Biocompatible tests for derived polymers. *Mater Today Commun* **2019**, *19*, 306-314. DOI: 10.1016/j.mtcomm.2019.02.007.

(14) Ji, H. Y.; Chen, X. L.; Wang, B.; Pan, L.; Li, Y. S. Metal-free, regioselective and stereoregular alternating copolymerization of monosubstituted epoxides and tricyclic anhydrides. *Green Chem* **2018**, *20* (17), 3963-3973. DOI: 10.1039/c8gc01641k.

(15) Li, D. S.; Sha, K.; Li, Y. P.; Wang, S. W.; Wang, J. Y. Synthesis and characterization of triblock copolymer by combining enzymatic condensation polymerization and ATRP. *Chinese Sci Bull* **2006**, *51* (9), 1065-1068. DOI: 10.1007/s11434-006-1065-9.

(16) Wang, L. J.; Wang, F.; Zhou, Q.; Wang, Y. F.; Song, H. X.; Yang, H. Y. Metal-free Lewis pairs catalysed synthesis of fluorescently labelled polyester-based amphiphilic polymers for biological imaging. *Eur Polym J* **2022**, *166*. DOI: 10.1016/j.eurpolymj.2022.111033.

(17) Xie, R.; Zhang, Y. Y.; Yang, G. W.; Zhu, X. F.; Li, B.; Wu, G. P. Record Productivity and Unprecedented Molecular Weight for Ring-Opening Copolymerization of Epoxides and Cyclic Anhydrides Enabled by Organoboron Catalysts. *Angewandte Chemie International Edition* **2021**, *60* (35), 19253-19261. DOI: 10.1002/anie.202104981.

(18) Abel, B. A.; Lidston, C. A. L.; Coates, G. W. Mechanism-Inspired Design of Bifunctional Catalysts for the Alternating Ring-Opening Copolymerization of Epoxides and Cyclic Anhydrides. *J Am Chem Soc* **2019**, *141* (32), 12760-12769. DOI: 10.1021/jacs.9b05570.

(19) Deacy, A. C.; Gregory, G. L.; Sulley, G. S.; Chen, T. T. D.; Williams, C. K. Sequence Control from Mixtures: Switchable Polymerization Catalysis and Future Materials Applications. *J Am Chem Soc* **2021**, *143* (27), 10021-10040. DOI: 10.1021/jacs.1c03250   From NLM PubMed-not-MEDLINE. Gregory, G. L.; Williams, C. K. Exploiting Sodium Coordination in Alternating Monomer Sequences to Toughen Degradable Block Polyester Thermoplastic Elastomers. *Macromolecules* **2022**, *55* (6), 2290-2299. DOI: 10.1021/acs.macromol.2c00068   From NLM PubMed-not-MEDLINE. Snyder, R. L.;

Lidston, C. A. L.; De Hoe, G. X.; Parvulescu, M. J. S.; Hillmyer, M. A.; Coates, G. W. Mechanically robust and reprocessable imine exchange networks from modular polyester pre-polymers. *Polym Chem-Uk* **2020**, *11* (33), 5346-5355. DOI: 10.1039/c9py01957j.

(20) Lidston, C. A. L.; Severson, S. M.; Abel, B. A.; Coates, G. W. Multifunctional Catalysts for Ring-Opening Copolymerizations. *ACS Catalysis* **2022**, *12* (18), 11037-11070. DOI: 10.1021/acscatal.2c02524.

(21) Rostamian, M.; Kalaee, M. R.; Dehkordi, S. R.; Panahi-Sarmad, M.; Tirgar, M.; Goodarzi, V. Design and characterization of poly(glycerol-sebacate)-co-poly (caprolactone) (PGS-co-PCL) and its nanocomposites as novel biomaterials: The promising candidate for soft tissue engineering. *Eur Polym J* **2020**, *138*. DOI: 10.1016/j.eurpolymj.2020.109985. Rabnawaz, M.; Wyman, I.; Auras, R.; Cheng, S. A roadmap towards green packaging: the current status and future outlook for polyesters in the packaging industry. *Green Chem* **2017**, *19* (20), 4737-4753. DOI: 10.1039/c7gc02521a.

(22) Zhu, Y. Z.; Shen, J.; Yin, L.; Wei, X. J.; Chen, F.; Zhong, M. Q.; Gu, Z.; Xie, Y.; Jin, W.; Liu, Z. J.; et al. Directly photopatterning of polycaprolactone-derived photocured resin by UV-initiated thiol-ene "click" reaction: Enhanced mechanical property and excellent biocompatibility. *Chem Eng J* **2019**, *366*, 112-122. DOI: 10.1016/j.cej.2019.02.045.

(23) Sanford, M. J.; Carrodeguas, L. P.; Van Zee, N. J.; Kleij, A. W.; Coates, G. W. Alternating Copolymerization of Propylene Oxide and Cyclohexene Oxide with Tricyclic Anhydrides: Access to Partially Renewable Aliphatic Polyesters with High Glass Transition Temperatures. *Macromolecules* **2016**, *49* (17), 6394-6400. DOI: 10.1021/acs.macromol.6b01425.

(24) Liang, J. X.; Ye, S. X.; Wang, S. Y.; Wang, S. J.; Han, D. M.; Huang, S.; Huang, Z. H.; Liu, W.; Xiao, M.; Sun, L. Y.; et al. Biodegradable Copolymers from CO2, Epoxides, and Anhydrides Catalyzed by Organoborane/Tertiary Amine Pairs: High Selectivity and Productivity. *Macromolecules* **2022**, *55* (14), 6120-6130. DOI: 10.1021/acs.macromol.2c01118.

(25) Ding, X.; Wu, Y. L.; Gao, J.; Wells, A.; Lee, K.; Wang, Y. Tyramine functionalization of poly(glycerol sebacate) increases the elasticity of the polymer. *J Mater Chem B* **2017**, *5* (30), 6097-6109. DOI: 10.1039/C7TB01078H.

(26) Chen, Y.; Miller, P. G.; Ding, X. C.; Stowell, C. E. T.; Kelly, K. M.; Wang, Y. D. Chelation Crosslinking of Biodegradable Elastomers. *Adv Mater* **2020**, *32* (43). DOI: 10.1002/adma.202003761.

(27) Ding, X.; Chen, Y.; Chao, C. A.; Wu, Y. L.; Wang, Y. Control the Mechanical Properties and Degradation of Poly(Glycerol Sebacate) by Substitution of the Hydroxyl Groups with Palmitates. *Macromol Biosci* **2020**, *20* (9), e2000101. DOI: 10.1002/mabi.202000101.

(28) Gockler, T.; Haase, S.; Kempter, X.; Pfister, R.; Maciel, B. R.; Grimm, A.; Molitor, T.; Willenbacher, N.; Schepers, U. Tuning Superfast Curing Thiol-Norbornene-Functionalized Gelatin Hydrogels for 3D Bioprinting. *Adv Healthc Mater* **2021**, *10* (14). DOI: 10.1002/adhm.202100206.

(29) Yeh, Y. C.; Ouyang, L. L.; Highley, C. B.; Burdick, J. A. Norbornene-modified poly(glycerol sebacate) as a photocurable and biodegradable elastomer. *Polym Chem-Uk* **2017**, *8* (34), 5091-5099. DOI: 10.1039/c7py00323d.

(30) Ligon, S. C.; Liska, R.; Stampfl, J.; Gurr, M.; Mulhaupt, R. Polymers for 3D Printing and Customized Additive Manufacturing. *Chem Rev* **2017**, *117* (15), 10212-10290. DOI: 10.1021/acs.chemrev.7b00074.

(31) Oesterreicher, A.; Gorsche, C.; Ayalur-Karunakaran, S.; Moser, A.; Edler, M.; Pinter, G.; Schlogl, S.; Liska, R.; Griesser, T. Exploring Network Formation of Tough and Biocompatible Thiol-yne Based Photopolymers. *Macromol Rapid Comm* **2016**, *37* (20), 1701-1706. DOI: 10.1002/marc.201600369.

(32) Tan, H. Y.; Trier, S.; Rahbek, U. L.; Dufva, M.; Kutter, J. P.; Andresen, T. L. A multi-chamber microfluidic intestinal barrier model using Caco-2 cells for drug transport studies. *PLoS One* **2018**, *13* (5), e0197101. DOI: 10.1371/journal.pone.0197101. Sticker, D.; Geczy, R.; Hafeli, U. O.; Kutter, J. P.

Thiol-Ene Based Polymers as Versatile Materials for Microfluidic Devices for Life Sciences Applications. *ACS Appl Mater Interfaces* **2020**, *12* (9), 10080-10095. DOI: 10.1021/acsami.9b22050.

(33) Lang, K.; Davis, L.; Torres-Kolbus, J.; Chou, C.; Deiters, A.; Chin, J. W. Genetically encoded norbornene directs site-specific cellular protein labelling via a rapid bioorthogonal reaction. *Nat Chem* **2012**, *4* (4), 298-304. DOI: 10.1038/nchem.1250.

(34) Jimenez-Quero, A.; Pollet, E.; Zhao, M.; Marchioni, E.; Averous, L.; Phalip, V. Itaconic and Fumaric Acid Production from Biomass Hydrolysates by Aspergillus Strains. *J Microbiol Biotechnol* **2016**, *26* (9), 1557-1565. DOI: 10.4014/jmb.1603.03073.

(35) Constant, E.; King, O.; Weems, A. C. Bioderived 4D Printable Terpene Photopolymers from Limonene and beta-Myrcene. *Biomacromolecules* **2022**, *23* (6), 2342-2352. DOI: 10.1021/acs.biomac.2c00085.

(36) Sticker, D.; Geczy, R.; Hafeli, U. O.; Kutter, J. P. Thiol-Ene Based Polymers as Versatile Materials for Microfluidic Devices for Life Sciences Applications. *Acs Appl Mater Inter* **2020**, *12* (9), 10080-10095. DOI: 10.1021/acsami.9b22050.

(37) Lee, K. Y.; Peters, M. C.; Anderson, K. W.; Mooney, D. J. Effect of mechanical stimulation on growth factor release from synthetic extracellular matrices. *Abstr. Pap. - Am. Chem. Soc.* **2001**, *221st*, MSE-499.

(38) Brooks, S. L.; Arno, M. C.; Dove, A. P.; Weems, A. C. Postfabrication Functionalization of 4D-Printed Polycarbonate Photopolymer Scaffolds. *ACS Applied Polymer Materials* **2022**, *4* (8), 5670-5679. DOI: 10.1021/acsapm.2c00648. Brooks, S. L.; Constant, E. J.; King, O. M.; Weems, A. C. Stereochemistry and stoichiometry in aliphatic polyester photopolymers for 3D printing tailored biomaterial scaffolds. *Polym Chem-Uk* **2022**, *13* (14), 2048-2056, 10.1039/D1PY01405F. DOI: 10.1039/D1PY01405F. Merckle, D.; Constant, E.; Cartwright, Z.; Weems, A. C. Ring Opening

Copolymerization of Four-Dimensional Printed Shape Memory Polyester Photopolymers Using Digital Light Processing. *Macromolecules* **2021**, *54* (6), 2681-2690. DOI: 10.1021/acs.macromol.0c02401.

(39) Chen, L.; Wu, Q.; Wei, G.; Liu, R.; Li, Z. Highly stable thiol–ene systems: from their structure–property relationship to DLP 3D printing. *Journal of Materials Chemistry C* **2018**, *6* (43), 11561-11568, 10.1039/C8TC03389G. DOI: 10.1039/C8TC03389G. Leonards, H.; Engelhardt, S.; Hoffmann, A.; Pongratz, L.; Schriever, S.; Bläsius, J.; Wehner, M.; Gillner, A. *Advantages and drawbacks of Thiol-ene based resins for 3D-printing*; SPIE, 2015.

(40) Walker, J. M.; Bodamer, E.; Krebs, O.; Luo, Y.; Kleinfehn, A.; Becker, M. L.; Dean, D. Effect of Chemical and Physical Properties on the In Vitro Degradation of 3D Printed High Resolution Poly(propylene fumarate) Scaffolds. *Biomacromolecules* **2017**, *18* (4), 1419-1425. DOI: 10.1021/acs.biomac.7b00146 From NLM Medline. Mondschein, R. J.; Kanitkar, A.; Williams, C. B.; Verbridge, S. S.; Long, T. E. Polymer structure-property requirements for stereolithographic 3D printing of soft tissue engineering scaffolds. *Biomaterials* **2017**, *140*, 170-188. DOI: 10.1016/j.biomaterials.2017.06.005.

(41) Chiou, B.-S.; English, R. J.; Khan, S. A. Rheology and Photo-Cross-Linking of Thiol−Ene Polymers. *Macromolecules* **1996**, *29* (16), 5368-5374. DOI: 10.1021/ma960383e.

(42) Luo, Y. Y.; Le Fer, G.; Dean, D.; Becker, M. L. 3D Printing of Poly(propylene fumarate) Oligomers: Evaluation of Resin Viscosity, Printing Characteristics and Mechanical Properties. *Biomacromolecules* **2019**, *20* (4), 1699-1708. DOI: 10.1021/acs.biomac.9b00076.

(43) Fritschen, A.; Bell, A. K.; Konigstein, I.; Stuhn, L.; Stark, R. W.; Blaeser, A. Investigation and comparison of resin materials in transparent DLP-printing for application in cell culture and organs-on-a-chip. *Biomater Sci* **2022**, *10* (8), 1981-1994. DOI: 10.1039/d1bm01794b.

(44) Kinstlinger, I. S.; Saxton, S. H.; Calderon, G. A.; Ruiz, K. V.; Yalacki, D. R.; Deme, P. R.; Rosenkrantz, J. E.; Louis-Rosenberg, J. D.; Johansson, F.; Janson, K. D.; et al. Generation of model tissues

with dendritic vascular networks via sacrificial laser-sintered carbohydrate templates (vol 4, pg 916, 2020). *Nat Biomed Eng* **2021**, *5* (8), 941-941. DOI: 10.1038/s41551-021-00761-6.

The authors declare no conflict of interest.

Click here to access/download
Supplementary file
ACS_supporting_info-3.pdf

This work made no use of animal studies or human research participants. Ethics approval and consent to participate therefore do not apply.